Doping phase diagram of a Hubbard model for twisted bilayer cuprates

Xiancong Lu[1] and D. Sénéchal[2]
[1]*Department of Physics, Xiamen University, Xiamen 361005, China*
[2]*Département de physique and Institut quantique, Université de Sherbrooke, Sherbrooke, Québec J1K 2R1, Canada*

(Received 1 December 2021; revised 9 June 2022; accepted 10 June 2022; published 21 June 2022)

We study the twisted Hubbard model of a cuprate bilayer at a fixed twist angle $\theta = 53.13^\circ$ and as a function of doping, using the variational cluster approximation, a method that treats short-range dynamical correlations exactly. At intermediate interlayer tunneling, we observe a sudden change of the relative sign of the d-wave order parameters of two layers between the underdoped and overdoped regimes. At strong interlayer tunneling, we observe a clear time-reversal symmetry breaking phase near optimal doping, in which the relative phase of the two layers changes continuously from 0 to π. However, this phase has trivial topology. We also apply a cluster extension of dynamical mean field theory to the same problem, but fail to detect a time-reversal breaking phase with that method, probably owing to the very small energy difference between the different states involved.

DOI: 10.1103/PhysRevB.105.245127

I. INTRODUCTION

The experimental discovery of correlated insulators and unconventional superconductivity in twisted bilayer graphene (TBG) [1,2] has opened up the new field of twistronics [3,4]. By twisting two graphene sheets by a small relative angle, a long-period moiré pattern forms in the bilayer. At special *magic* angles, the moiré band structure of TBG exhibits isolated flat bands near charge neutrality [5–7], which lead to a variety of strongly correlated phenomena. Following this discovery, various twisted van der Waals heterostructures have been constructed and investigated [8], including transition metal dichalcogenides [9–12], double bilayer graphene [13–15], and trilayer graphene [16–19].

Recently, twistronics concepts have been extended to high-temperature superconductors [20,21], which are strongly correlated materials by themselves. This was motivated by the experimental realization of two-dimensional (2D) monolayer $Bi_2Sr_2CaCu_2O_{8+\delta}$ (Bi2212), whose transition temperature is shown to be very close to that of bulk samples [22,23]. It is theoretically predicted that, at large twist angles (close to 45°), a fully gapped $d + id$ superconducting phase emerges, which spontaneously breaks time-reversal symmetry (TRS) and is topologically nontrivial [20]. This TRS breaking superconducting phase is also predicted to be stable at small twist angle, due to the strong renormalization of Bogoliubov-de Gennes (BdG) quasiparticles near the nodes [21]. In order to determine the pairing symmetry of cuprate superconductors, c-axis twisted Josephson junctions, formed by stacking two Bi2212 crystals along the c axis, have been realized [24–29]. However, most experimental works did not observe the angular dependence of the Josephson current [24,25,29]. Owing to the novel technique of van der Waals stacking, high-quality twisted Bi2212 Josephson junctions with an atomically sharp interface have been successfully fabricated recently [29,30].

Previous theoretical work on twisted bilayer cuprates are mainly based on Bogoliubov-de-Gennes mean-field theory [20,21,28,31,32], which does not take into account the effects of strong correlations. To overcome this, a twisted t-J model of cuprates has been proposed and studied within slave-boson mean-field theory [33], in which a topological-trivial time-reversal symmetry breaking superconductor is also found, but within a small range of twist angles around 45°, questioning the possibility of topological superconductors in this region. In spite of this work, the stability of the novel superconducting phases against doping has not been fully addressed before in the literature. In this paper, we will numerically study the twisted Hubbard model of bilayer cuprates using the variational cluster approach (VCA) and cluster dynamical mean field theory (CDMFT). These approaches have been successfully used in the past to study high-temperature superconductors and the Hubbard model at intermediate coupling is arguably a better representation of these materials. We will focus on a fixed twisted angle $\theta = 53.13^\circ$, at which these cluster methods are easily applicable, and investigate the superconducting phase diagram as a function of doping for two different sets of interlayer tunneling.

This paper is organized as follows. In Sec. II, we introduce the Hubbard model for the twisted bilayer. In Sec. III, we review the variational cluster approximation (VCA) and present our main results obtained from this method, e.g., the phase diagram of bilayer as a function of hole doping. In Sec. IV we refine the VCA analysis by adding interlayer pairing as variational parameters. In Sec. V, we present the corresponding results from cluster dynamical mean field theory (CDMFT).

II. MODEL

A. Hamiltonian

We assume that each of the two layers of the system can be described by the one-band Hubbard model (the sites correspond to the location of copper atoms). The bilayer is then described by the following tight-binding Hubbard

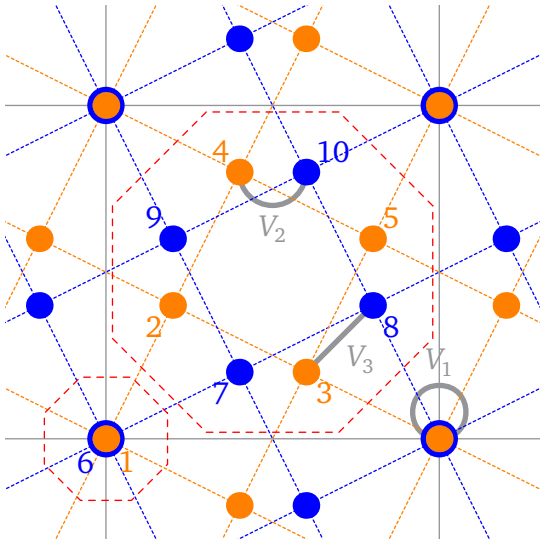

FIG. 1. Unit cell of the bilayer twisted by an angle $\theta = 2\arctan\frac{1}{2} = 53.13°$. The ten sites within the unit cell are labeled and their color (orange or blue) indicates the layer. The three most important interlayer tunneling terms ($V_{1,2,3}$) are illustrated in gray. (the red-dashed enclosures are the clusters used in VCA; see below).

model [20,33]:

$$H = H^{(1)} + H^{(2)} + H_\perp, \tag{1}$$

where the intralayer Hamiltonian $H^{(\ell)}$ is

$$H^{(\ell)} = \sum_{\mathbf{r},\mathbf{r}'\in\ell,\sigma} t_{\mathbf{r}\mathbf{r}'} c^\dagger_{\mathbf{r},\ell,\sigma} c_{\mathbf{r}',\ell,\sigma} + U \sum_{\mathbf{r}} n_{\mathbf{r},\ell,\uparrow} n_{\mathbf{r},\ell,\downarrow} - \mu \sum_{\mathbf{r},\sigma} n_{\mathbf{r},\ell,\sigma}, \tag{2}$$

where $c_{\mathbf{r},\ell,\sigma}$ ($c^\dagger_{\mathbf{r},\ell,\sigma}$) is the annihilation (creation) operator of an electron at site $\mathbf{r}$ on layer ℓ ($\ell = 1, 2$) with spin $\sigma = \uparrow, \downarrow$, and $n_{\mathbf{r},\ell,\sigma}$ is the associated number density operator. The labels $\mathbf{r}, \mathbf{r}'$ run over the possible sites of a square lattice (each layer has its own). We will keep nearest-neighbor (t) and next-nearest-neighbor (t') hopping terms only, so that the dispersion relation on a square lattice is $\varepsilon(\mathbf{k}) = -2t(\cos k_x + \cos k_y) + 4t' \cos k_x \cos k_y - \mu$. Only on-site interactions are considered here. For Bi2212, the nearest-neighbor hopping is $t = 126$ meV [34]. In the remainder of this paper, we set t as the energy unit, and choose the other parameters to be $t' = -0.3$ and $U = 8$.

The interlayer tunneling is represented by

$$H_\perp = \sum_{n=1}^{3} V_n \sum_{\langle \mathbf{r},\mathbf{r}'\rangle_{\perp,n},\sigma} [c^\dagger_{\mathbf{r},1,\sigma} c_{\mathbf{r}',2,\sigma} + \text{H.c.}], \tag{3}$$

where the notation $\langle \mathbf{r}, \mathbf{r}'\rangle_{\perp,n}$ ($n = 1, 2, 3$) stands for the set of square lattice sites $\mathbf{r}$ on layer 1 and $\mathbf{r}'$ on layer 2 such that their projection on the plane are nth neighbors. This is illustrated on Fig. 1 for V_1, V_2, and V_3. For instance, V_1 is the interlayer tunneling between sites located exactly on top of each other, V_2 for sites that are first neighbors when projected on a common plane, etc. Such an interlayer tunneling model is obviously oversimplified, as it ignores the complexity of the CuO_2 layers and of the rare-earth layers that will intervene between the twisted CuO_2 layers. In this paper we will use two sets of values for V_n, shown in Table I. These values can be fitted to the formula $V_i = t_\perp \exp(-\sqrt{d^2 + r_i^2}/a)$, where r_i is the lateral distance between sites involved in the interlayer hopping, d an interlayer distance and a a decay constant. Those of set II in Table I correspond to $t_\perp = 1.53t$, $a = 0.29$, and $d = 0.39$, the latter values being defined in units of the lattice spacing of each layer. These values have been chosen heuristically, those of set II being four times larger than those of set I and certainly unrealistic, but necessary in order to unravel TRS breaking, as we will see below. Given the accepted values of hopping along the c axis in bulk cuprates, even the values of set I are large, and will be referred to as *intermediate tunneling*, whereas those of set II will constitute *strong tunneling*.

TABLE I. The two sets of interlayer hopping terms used in this paper.

Set	V_1	V_2	V_3
I	0.1	0.05	0.03
II	0.4	0.2	0.12

In order to simplify as much as possible our numerical work, we will restrict our analysis to a twist angle of $\theta = 2\arctan\frac{1}{2} = 53.13°$. The unit cell of the twisted bilayer at that angle is illustrated on Fig. 1 and contains ten sites (five per layer).

B. Symmetries

The bilayer system is invariant under a $\pi/4$ rotation around the z axis (perpendicular to the bilayer plane) and under the π rotations C_x, C_y, C_d, and C'_d illustrated on Fig. 2, which make up the D_4 point group, the same as for an isolated layer. Possible superconducting gap functions for this system should in principle be classified according to the irreducible representations of D_4. Table II shows the character table and the simplest gap functions associated with each irreducible representation. Representations B_1 and B_2 correspond to what is usually called $d_{x^2-y^2}$ and d_{xy}, respectively. Representations A_1 and A_2 correspond respectively to s wave (or extended s wave) and f wave, and the two-dimensional representation

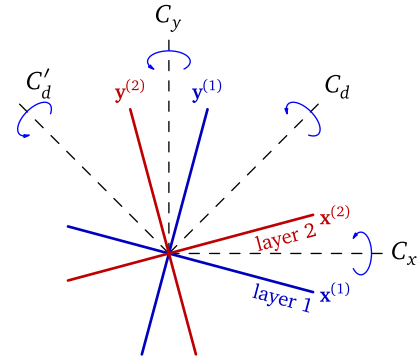

FIG. 2. Symmetries on the bilayer system. The axes of the two layers are indicated in blue and red, respectively. The rotations C_x, C_y, C_d, and C'_d are indicated; the rotations C_2 and C_4, within each plane, are not.

TABLE II. Character table of D_4, with a list of the simplest gap basis functions. The rotation C_d' is defined about the other diagonal axis, at right angle from C_d.

	e	$2C_4$	C_2	$C_{x,y}$	$C_{d,d'}$	Gap functions
A_1	1	1	1	1	1	1
A_2	1	1	1	−1	−1	$\sin k_x \ \sin k_y(\cos k_x - \cos k_y)$
B_1	1	−1	1	1	−1	$\cos k_x - \cos k_y$
B_2	1	− 1	1	− 1	1	$\sin k_x \ \sin k_y$
E	2	0	− 2	0	0	$(\sin k_x, \sin k_y)$

E would correspond to (triplet) p wave, with basis (p_x, p_y). Thus, the only possibility of a (pure) chiral representation is $p_x + ip_y$, a triplet state that will not occur in this cuprate system. We rather expect representations B_1 and B_2 to be realized here, owing to the d-wave character of superconductivity in single layers. In principle, according to the Landau theory of phase transitions, one of those two should prevail just below T_c, but there is always the possibility that, the two states (B_1 and B_2) being very close in energy, a second phase transition occurs below T_c and a complex combination $d_{x^2-y^2} + id_{xy}$ is present at zero temperature. This is the scenario anticipated in Ref. [20] and investigated here. Figure 3 illustrates representations B_1 and B_2 in terms of the phases (± 1) of the superconducting pairings on nearest-neighbor links, for the specific case of the 53° twist angle. This twist can also be regarded from the complementary angle $\pi/2 - \theta = 37°$. In the B_1 representation, links separated by the large angle (53°) have the same sign, whereas in the B_2 representation this holds for links separated by the small angle (37°).

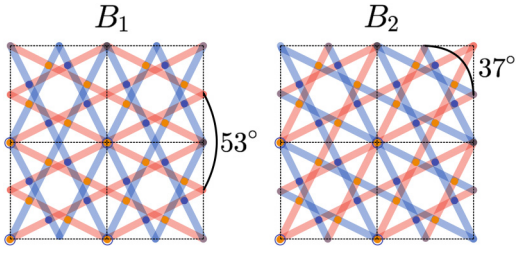

FIG. 3. Schematics of pairing in representations B_1 and B_2 for the 53° twist angle. Pairing occurs on links, blue and red mean positive and negative amplitudes, respectively. In the B_1 representation, links with the same pairing sign are separated by 53°. In the B_2 representation, they are separated by the complementary angle 37°.

III. RESULTS FROM THE VARIATIONAL CLUSTER APPROXIMATION

High-temperature superconductors have strong correlations. There is a limited number of numerical methods that can tackle such systems, and methods based on small clusters of sites embedded into an effective medium are amongst the most successful. These so-called *quantum cluster methods* are approximation strategies for the electron Green function $G(\mathbf{k}, \omega)$, by which the electron self-energy Σ on the infinite lattice is approximated by that of a small cluster. In this paper we will apply two of these methods to the bilayer Hamiltonian (1).

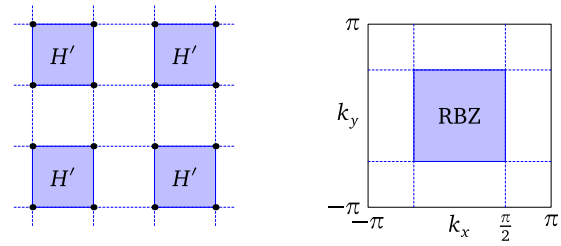

FIG. 4. Schematics of cluster methods. Left panel: The lattice is tiled into identical 2×2 clusters with Hamiltonian H'. Right panel: The reduced Brillouin zone (RBZ) is then four times smaller than the original Brillouin zone.

The first of these methods is the variational cluster approximation (VCA) [35–37]. It is based on a variational principle proposed by Potthoff [35] and can be seen as a variational extension of cluster perturbation theory (CPT) [38,39]. Let us start by briefly summarizing the latter. In CPT, the lattice is tiled into identical *clusters*, and the Hamiltonian is written as $H = H' + V$, where H' is the restriction of H to the clusters and V only contains hopping terms between different clusters. If the model contains N_b bands and each cluster contains L lattice sites, then LN_b must be small enough to allow for an exact numerical solution of H', and the associated one-particle Green function $\mathbf{G}_c(\omega)$ on the cluster is a $2LN_b \times 2LN_b$ matrix (the factor of 2 because of spin). The tiling into clusters defines a superlattice, and the corresponding Brillouin zone is L times smaller than the original Brillouin zone (see Fig. 4). We call it the reduced Brillouin zone and its wave vectors are noted $\tilde{\mathbf{k}}$. The hopping matrix in H can be expressed as a $2LN_b \times 2LN_b$ matrix $\mathbf{t}(\tilde{\mathbf{k}})$, a function of $\tilde{\mathbf{k}}$, which is the sum of a $\tilde{\mathbf{k}}$-independent part $\mathbf{t}_c$ and of the intercluster part $\mathbf{V}(\tilde{\mathbf{k}})$: $\mathbf{t}(\tilde{\mathbf{k}}) = \mathbf{t}_c + \mathbf{V}(\tilde{\mathbf{k}})$. The self-energy $\mathbf{\Sigma}_c(\omega)$ associated with the cluster Green function $\mathbf{G}_c(\omega)$ is thus defined by Dyson's equation on the cluster:

$$\mathbf{G}_c^{-1} = \omega - \mathbf{t}_c - \mathbf{\Sigma}_c(\omega) \tag{4}$$

In CPT, the electron self-energy is approximated by that of the restriction H' of the Hamiltonian to the cluster. In the mixed momentum-cluster site basis, the electron Green function is then given by the following relation:

$$\mathbf{G}^{-1}(\tilde{\mathbf{k}}, \omega) = \omega - \mathbf{t}(\tilde{\mathbf{k}}) - \mathbf{\Sigma}_c(\omega) = \mathbf{G}_c^{-1}(\omega) - \mathbf{V}(\tilde{\mathbf{k}}). \tag{5}$$

We assume here that the chemical potential μ is included in the hopping matrix $\mathbf{t}(\tilde{\mathbf{k}})$.

CPT is unable to describe broken symmetry states: It is not a self-consistent approach, nor is it based on a variational principle. The VCA adds a variational aspect to CPT: the cluster Hamiltonian H' is augmented by a certain number of *Weiss fields*:

$$H' \to H' + \sum_a h_a \hat{O}_a \tag{6}$$

where the operators $\hat{O}_a$ are defined on the cluster only, and possibly represent broken symmetries. These additional terms are in turn subtracted from V, so that the original

Hamiltonian H is unaffected. The values h_a of these Weiss fields are not arbitrary, but set by Potthoff's variational principle: The following function:

$$\Omega(h_a) = \Omega' - \int \frac{d\omega}{2\pi} \sum_{\tilde{\mathbf{k}}} \ln\det[\mathbf{1} - \mathbf{V}(\tilde{\mathbf{k}})\mathbf{G}_c(\omega)] \quad (7)$$

should be stationary with respect to these fields h_a. In that expression, Ω' is the ground-state energy of the cluster Hamiltonian H' and $\mathbf{G}_c(\omega)$ is the electron Green function derived from the cluster Hamiltonian H' that includes the Weiss fields $h_a\hat{O}_a$.

In the problem at hand, it might seem natural to use the 10-site unit cell shown in Fig. 1 as the repeated cluster, especially since 10 sites is an easily manageable size for an exact-diagonalization solver. However, the set of numbered sites in Fig. 1 does not have the D_4 symmetry of the full Hamiltonian, and this complicates the VCA computations [40] We will rather use a slight refinement of the method described above, assuming that the repeated unit is a *supercluster* of 10 sites obtained by assembling an octagonal cluster of 8 sites and a point-like cluster of 2 sites, each delimited by a red dashed line in Fig. 1. The self-energy of the supercluster is then a direct sum of the self-energies of an 8-site and of a 2-site cluster. Otherwise, the method is unchanged from the general approach described above. Although it might seem that the 2-site cluster plays little role in the computation, it is essential to properly tile the lattice model and its self-energy is nontrivial, even though it has no anomalous part; in particular, it contributes to the Mott character of the solutions at half-filling.

On the octagonal cluster, we will define Weiss fields associated with d-wave superconductivity on each layer. On each layer of the lattice, we can define an operator field that describes d-wave superconductivity:

$$\hat{\Delta}^{(\ell)} = \sum_{\mathbf{r}\in\ell} \{c_{\mathbf{r},\ell,\uparrow} c_{\mathbf{r}+\mathbf{x}^{(\ell)},\ell,\downarrow} - c_{\mathbf{r},\ell,\downarrow} c_{\mathbf{r}+\mathbf{x}^{(\ell)},\ell,\uparrow} - c_{\mathbf{r},\ell,\uparrow} c_{\mathbf{r}+\mathbf{y}^{(\ell)},\ell,\downarrow} + c_{\mathbf{r},\ell,\downarrow} c_{\mathbf{r}+\mathbf{y}^{(\ell)},\ell,\uparrow}\} \quad (8)$$

where $\mathbf{x}^{(\ell)}$ and $\mathbf{y}^{(\ell)}$ are the orthogonal lattice vectors on layer ℓ (see Fig. 2). These operators do not fall into the irreducible representations of Table II, but the following combinations do:

$$\hat{B}_1 = \hat{\Delta}^{(1)} + \hat{\Delta}^{(2)} \quad \hat{B}_2 = \hat{\Delta}^{(1)} - \hat{\Delta}^{(2)} \quad (9)$$

(we use the same symbols for the operators and the associated irreducible representations, hoping that the context will dissipate any ambiguity between the two).

To each of these operators we associate an order parameter, the average of the operator per site: $B_i = \langle\hat{B}_i\rangle/N$ and $\Delta^{(i)} = \langle\hat{\Delta}^{(i)}\rangle/N$, N being the total number of sites (atoms). These order parameters are in general complex and have a phase $\phi^{(i)} = \arg\Delta^{(i)}$. The relative phase ϕ between the d-wave operators on the two layers is then defined as $\phi = \phi^{(1)} - \phi^{(2)}$. It is always possible to set the phase of B_1 to zero (hence $\mathrm{Im}\, B_1 = 0$) and, in the coexistence phase $d_{x^2-y^2} + id_{xy}$, we have correspondingly $\mathrm{Re}\, B_2 = 0$. It is then a simple matter to show from Eq. (9) that

$$\tan\frac{\phi}{2} = \frac{\mathrm{Im}\, B_2}{\mathrm{Re}\, B_1} \quad (10)$$

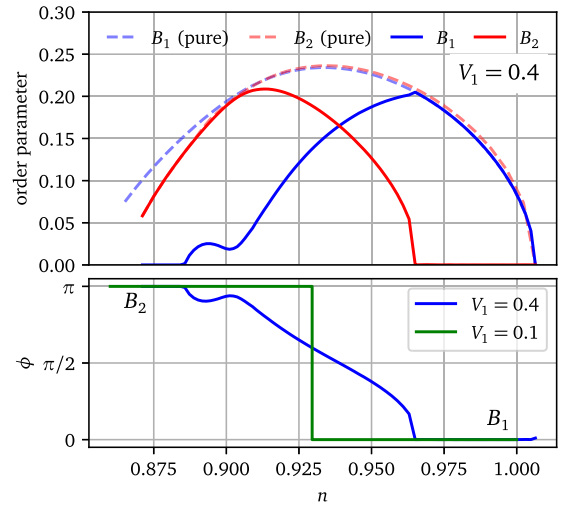

FIG. 5. Top panel: Order parameter as a function of electron density n, as obtained in VCA, for interlayer hopping set II. The dashed blue (red) curve is obtained when only the B_1 (B_2) representation is allowed. The full curves are obtained by allowing these two representations to coexist, leading to a TRS breaking phase when they do. Lower panel: The corresponding relative phase ϕ of the order parameters on the two layers. At intermediate interlayer hopping, the system jumps from $\phi = 0$ to $\phi = \pi$ at $n \approx 0.93$. At strong interlayer hopping, the switch is gradual.

The value $\phi = 0$ corresponds to the pure B_1 case (the links separated by 53° are in phase), and $\phi = \pi$ to the pure B_2 case (the links separated by 53° are in antiphase). Note that looking at the system as a twist of 37° instead would exchange these two pictures, because of the d-wave nature of superconductivity on each layer; thus the phase ϕ only has physical meaning modulo π.

Given the definition (9) We can add the following combinations to the cluster Hamiltonian:

$$H' \to H' + \sum_{\ell=1,2} d_\ell \hat{B}_{\ell c} + \mathrm{H.c.} \quad (11)$$

where $\hat{B}_{\ell c}$ is a restriction to the cluster of the lattice operator (9) and d_ℓ is a complex amplitude. The real and imaginary parts of d_ℓ are then Weiss fields in the sense of the coefficients h_a of Eq. (6). Again, because of the overall phase symmetry, one can always assume that d_1 and d_2 are real when studying the two representations separately, and we can assume d_1 to be real and d_2 to be purely imaginary when the two representations are in coexistence.

We applied the VCA method on this cluster system, using the two sets of interlayer tunneling defined in Table I. In practice, this means computing the cluster Green function $\mathbf{G}_c(\omega)$ repeatedly while adjusting the Weiss fields d_ℓ so as to make the Potthoff functional stationary (in fact, minimum). Once the stationary values are found, the Green function (5) can be used to compute the ground-state average of any one-body operator, in particular the order parameters B_1 and B_2. The electron density n can be likewise computed from the Green function (the chemical potential μ is the actual control parameter that is varied).

Figure 5 (top panel) shows the order parameter $|B_{1,2}|$ as a function of electron density n for hole doping at strong interlayer tunneling. The dashed curves are obtained by studying the two representations B_1 and B_2 independently. By contrast, the full curves are obtained by allowing coexistence between the two phases. For the pure phases, we note the characteristic dome shape that is typically obtained in quantum cluster methods, qualitatively agreeing with the known properties of cuprates. The electron density computed from the Green function (5) has some systematic error, as can be seen from the fact that the order parameter vanishes not at $n = 1$, as it should from Mott physics, but at $n = 1.006$. In the coexistence phase, the value of the Potthoff functional as a function of chemical potential $\Omega(\mu)$ is lower than those obtained in either of the two pure phases. The values of $\Omega(\mu)$ for the two pure phases cross near the point where the two phases are equal in magnitude, near $n = 0.94$.

The bottom panel of the figure shows the relative phase ϕ of the d-wave order parameters on the two layers [Eq. (10)]. It is either 0 or π in the pure phases, and interpolates between them in the coexistence region. At intermediate interlayer tunneling ($V_1 = 0.1$), the coexistence region is too narrow to be visible, and the phase switches abruptly from 0 at low doping (B_1 representation) to π at high doping (B_2 representation) at about $n \approx 0.93$. There is thus a doping-induced transition of the bilayer superconducting state, which coincides with the passage from underdoped to overdoped, judging by the location of optimal doping on the upper panel of the figure.

A more detailed view of how this is happening from the VCA perspective is shown on Fig. 6. On the top half of the figure, we show the profile of the Potthoff functional (7) as a function of the relative phase ϕ. For $n = 0.89$ and $n = 0.91$, the minimum is at $\phi = \pm\pi$ (B_2 representation). Near $n = 0.93$, the profile changes suddenly to one where the minimum is at $\phi = 0$ (B_1 representation). Note that the vertical scale is tiny (10^{-5}), in multiples of t, which defines the energy unit here. This means that the energy difference between the two representations B_1 and B_2 might just be too small to be of consequence experimentally ($\sim 10^{-2}$ meV or $\sim 10^{-1}$ K in terms of temperature), at an intermediate interlayer tunneling of $V_1 = 0.1$.

On the bottom half of Fig. 6, the same type of data is shown at strong interlayer tunneling ($V_1 = 0.4$). There the transition between B_2 and B_1 is gradual as the position of the minimum moves continuously from $\phi = \pm\pi$ to $\phi = 0$, with a spontaneous breaking of the $\phi \to -\phi$ symmetry. Even though this TRS breaking state is what we are looking for, such a strong value of interlayer tunneling is unrealistic.

Does this TRS breaking state have nontrivial topology? In a strongly correlated system, this question may be answered through the properties of the approximate interacting Green function (5) [41,42]. The key idea is to define a "topological Hamiltonian" $h_t(\mathbf{k}) = -G^{-1}(\mathbf{k}, \omega = 0)$, which can be diagonalized:

$$h_t(\mathbf{k})|\alpha, \mathbf{k}\rangle = \mu_\alpha(\mathbf{k})|\alpha, \mathbf{k}\rangle \tag{12}$$

One can then define a generalized Chern number just like in noninteracting systems:

$$C_1 = \int \frac{d^2k}{2\pi}\, \mathcal{F}_{xy}(\mathbf{k}) \quad \mathcal{F}_{xy}(\mathbf{k}) = \frac{\partial \mathcal{A}_y}{\partial k_x} - \frac{\partial \mathcal{A}_x}{\partial k_y} \tag{13}$$

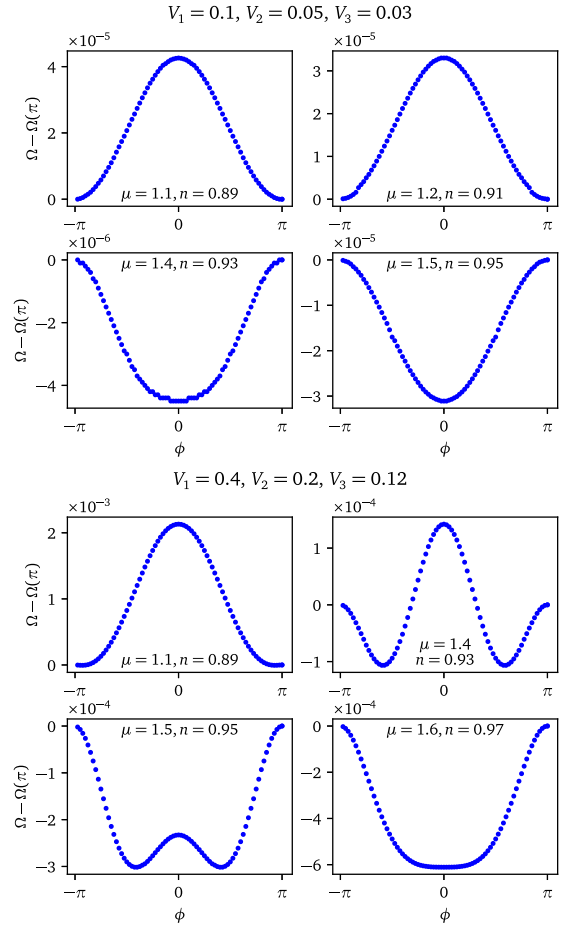

FIG. 6. Potthoff functional as a function of interlayer phase ϕ, for different values of the chemical potential, for intermediate (top) and strong (bottom) interlayer tunneling.

with the Berry connection

$$\mathcal{A}_j(\mathbf{k}) = -i \sum_{\mu_\alpha(\mathbf{k})<0} \langle \alpha, \mathbf{k}|\partial_{k_j}|\alpha, \mathbf{k}\rangle, \quad (j = x, y). \tag{14}$$

When applying this formula to the TRS states found by VCA, we find the topology to be trivial (the Chern number vanishes). This results from a compensation between different regions of the Brillouin zone, with opposite Berry curvature.

IV. INTERLAYER PAIRING IN VCA

In this section we bring refinements to our VCA analysis by adding variational parameters based on interlayer pairing. interlayer pairing operators too fall in irreducible representations of D_{4h}. Much like the interlayer hopping operators $V_{1,2,3}$, they can be defined for each lateral distance $d_\parallel$. Let us first define elementary singlet pairing operators between sites i and j as $\hat{\Delta}_{ij} = c_{i,\uparrow}c_{j,\downarrow} - c_{i,\downarrow}c_{j,\uparrow}$. In terms of these, we define the following interlayer pairing operators, here conveniently defined in the unit cell using the orbital numbering shown in Fig. 1:

$$\hat{A}_1^{1\perp} = \hat{\Delta}_{16}, \tag{15}$$

$$\hat{A}_1^{2\perp} = \hat{\Delta}_{4,10} + \hat{\Delta}_{3,7} + \hat{\Delta}_{2,9} + \hat{\Delta}_{5,8}, \tag{16}$$

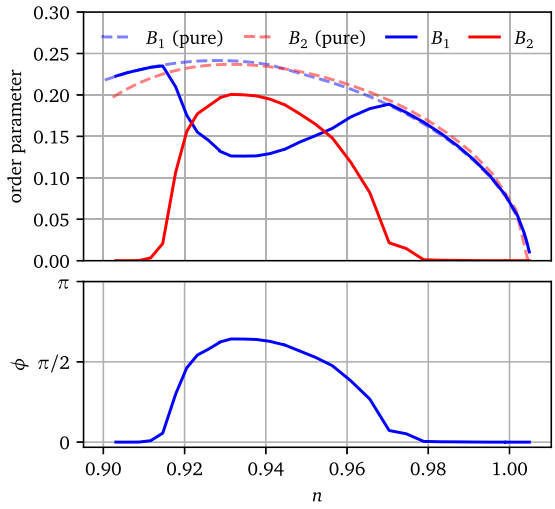

FIG. 7. Same as Fig. 5, but with solutions using 4 Weiss fields: the real parts of $\hat{B}_1$ and $\hat{B}_1^{2\perp}$, and the imaginary parts of $\hat{B}_2$ and $\hat{B}_2^{3\perp}$.

$$\hat{A}_1^{3\perp} = \hat{\Delta}_{2,7} + \hat{\Delta}_{5,10} + \hat{\Delta}_{4,9} + \hat{\Delta}_{3,8}, \tag{17}$$

$$\hat{B}_1^{2\perp} = \hat{\Delta}_{4,10} + \hat{\Delta}_{3,7} - \hat{\Delta}_{2,9} - \hat{\Delta}_{5,8}, \tag{18}$$

$$\hat{B}_2^{3\perp} = \hat{\Delta}_{2,7} + \hat{\Delta}_{5,10} - \hat{\Delta}_{4,9} - \hat{\Delta}_{3,8}. \tag{19}$$

The symbol of each operator indicates the D_{4h} representation, and the superscript indicates the neighbor (1st, 2nd, etc.), like for the interlayer tunneling amplitudes $V_{1,2,3}$. Even though these operators are defined within the unit cell with this notation, this is naturally extended to the whole lattice, since sites indices within the unit cell are in practice orbital indices for the full lattice.

Naturally, we expect these operators to have nonzero expectation values in a superconducting state within the same irreducible representation, even if they are not used as VCA Weiss fields, just because pairing correlations propagate from the cluster self-energy via the hopping terms of the model (both within and between clusters). In other words, interlayer pairing is present in our solutions even when it is not explicitly used to expand the set of VCA variational parameters. Explicitly, we verified that the expectations values $\langle A_1^{i\perp}\rangle$ $(i = 1, 2, 3)$ vanish in the superconducting states with B_1 or B_2 symmetry, and so forth.

However, it is tempting increase the variational space using these operators. For instance, when probing a solution in the B_1 representation, we could supplement the cluster Hamiltonian with two Weiss fields:

$$H' \to H' + d_1 \hat{B}_{1c} + d_1^{\perp} \hat{B}_1^{2\perp} + \text{H.c.} \tag{20}$$

and likewise for solutions in the B_2 representation, or mixed solutions belonging to $d_{x^2-y^2} + id_{xy}$.

Figure 7 shows the results of applying the VCA with four independent Weiss fields: the same two as in Fig. 5, plus two interlayer pairing operators: the real part of $\hat{B}_1^{2\perp}$, and the imaginary part of $\hat{B}_2^{3\perp}$. As we can see, there still is a TRS breaking phase, between $n = 0.91$ and $n = 0.98$. However, in contrast to the results presented in Fig. 5, the representation B_1 seems to win on both sides of this coexistence dome. This defies our intuition, gained from Sec. III that the coexistence phase is the result of a single-energy crossing between the B_1 and the B_2 phase as doping increases. A possible reason for this discrepancy is that the two representations B_1 and B_2 are not exactly treated on the same footing here. Whereas operators $\hat{B}_1$ and $\hat{B}_2$ are defined from the same sites and differ only by the signs of some pairings, operators $\hat{B}_1^{2\perp}$ and $\hat{B}_2^{3\perp}$ are not defined from the same sites. There is no interlayer singlet pairing operator belonging to B_2 defined from the pairings involved in $\hat{B}_1^{2\perp}$, and vice versa. Given the very small energy difference between the B_1 and B_2 solutions, this may be enough to bias the results and eliminate the small energy advantage that the B_2 representation had at higher doping.

Another reason to prefer the results of Fig. 5 is that we naturally expect representation B_2 to dominate at large doping. Indeed, in this representation, the pairing amplitudes on links separated by the small angle (37°) have the same sign—see Fig. 3—as we would naturally expect for small angles in a weakly correlated system, and at large doping the system becomes weakly correlated.

This lowers the degree of confidence we have in using interlayer pairing operators as additional VCA Weiss fields. Note that the expectation values $\langle \hat{B}_1^{2\perp}\rangle$ has the same order of magnitude whether the corresponding operator is used as an additional Weiss field or not. Again, we insist that the motivation for additional Weiss fields is strictly to increase the variational space and access to slightly lower-energy solutions, not actually allow interlayer pairing, which occurs anyway in the solutions of Sec. III.

V. RESULTS FROM CLUSTER DYNAMICAL MEAN FIELD THEORY

In order to test the robustness of our predictions, we have also studied the same system using cluster dynamical mean field theory (CDMFT) [43–46] with an exact diagonalization solver at zero temperature (or ED-CDMFT). Here the Weiss fields of VCA are replaced by a bath of uncorrelated orbitals whose parameters are determined self-consistently. Because the presence of this bath increases the size of the problem, the cluster cannot be as large as in VCA and typically contains no more than 4 sites.

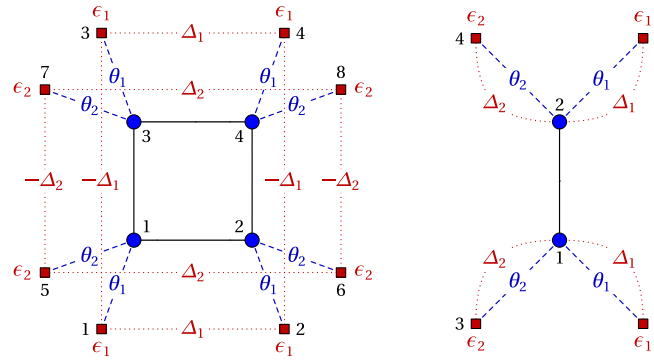

FIG. 8. Impurity models used in CDMFT. On the left, the 4-site cluster used for sites (2,3,4,5) and (7,8,9,10) of the unit cell, as labeled in Fig. 1. On the right, the 2-site cluster used for sites (1,6).

Each cluster, together with the associated bath, defines an Anderson impurity model (AIM):

$$H_{\rm imp} = H_c + \sum_{\mu,\alpha} \theta_{\mu,\alpha}(c^\dagger_\mu a_\alpha + \text{H.c.}) + \sum_{\alpha\beta} \epsilon_{\alpha\beta} a^\dagger_\alpha a_\beta \ , \quad (21)$$

where a_α annihilates an electron in the bath orbital labeled α. The Nambu formalism must be used to incorporate pairing between bath sites, within the matrix $\epsilon_{\alpha\beta}$, or within the hybridization $\theta_{\mu,\alpha}$, depending on the impurity model. The index μ then labels different sites of the cluster, together with the Nambu index, and takes $2L$ values in a cluster with L sites.

The bath parameters $\theta_{\mu,\alpha}$ and $\epsilon_{\alpha\beta}$ are determined by an approximate self-consistent procedure, as proposed initially in [47], that goes as follows: (i) Initial values of these parameters are chosen on the first iteration. (ii) For each iteration, the cluster Hamiltonian (21) is solved, i.e., the cluster Green function $\mathbf{G}_c(\omega)$ is computed. The latter can be expressed as

$$\mathbf{G}_c(\omega)^{-1} = \omega - \mathbf{t}_c - \mathbf{\Gamma}(\omega) - \mathbf{\Sigma}_c(\omega) \quad (22)$$

where $\mathbf{\Gamma}(\omega)$ is the bath hybridization matrix:

$$\Gamma_{ij}(\omega) = \sum_{\alpha,\alpha'} \theta_{i\alpha} \left(\frac{1}{\omega - \boldsymbol{\epsilon}} \right)_{\alpha\alpha'} \theta^*_{j\alpha'}. \quad (23)$$

(iii) The bath parameters are updated, by minimizing the distance function:

$$d(\boldsymbol{\epsilon}, \boldsymbol{\theta}) = \sum_{i\omega_n} W(i\omega_n)[\mathbf{G}_c(i\omega_n)^{-1} - \bar{\mathbf{G}}(i\omega_n)^{-1}] \quad (24)$$

where $\bar{\mathbf{G}}(\omega)$, the projected Green function, is defined as

$$\bar{\mathbf{G}}(\omega) = \frac{1}{N} \sum_{\mathbf{k}} \mathbf{G}(\mathbf{k}, \omega), \quad \mathbf{G}(\mathbf{k}, \omega) = \frac{1}{\omega - \mathbf{t}_\mathbf{k} - \mathbf{\Sigma}_c(\omega)} \ . \quad (25)$$

Ideally, $\bar{\mathbf{G}}(\omega)$ should coincide with the impurity Green function $\mathbf{G}_c(\omega)$, but the finite number of bath parameters does not allow for this correspondence at all frequencies, and so a distance function $d(\epsilon_r, \theta_{ir})$ is defined, with emphasis on low frequencies along the imaginary axis. The weight function $W(i\omega_n)$ is where the method has some arbitrariness; in this paper $W(i\omega_n)$ is taken to be a constant for all Matsubara frequencies lower than a cutoff $\omega_c = 2t$, with a fictitious temperature $\beta^{-1} = t/50$. (iv) We go back to step (ii) and iterate until the bath parameters or the bath hybridization function $\mathbf{\Gamma}(\omega)$ stop varying within some preset tolerance.

In the current problem, the 10-site unit cell was separated in three impurity problems: a 4-site cluster on each layer (which together are equivalent to the 8-site cluster used in VCA in the last section), made respectively of the orbitals (2,3,4,5) and (7,8,9,10) as labeled on Fig. 1, and a 2-site cluster made of orbitals (1,6). These clusters are illustrated on Fig. 8. The 4-site cluster is connected to 8 uncorrelated bath orbitals, and contains 6 independent parameters: Two bath energies $\epsilon_{1,2}$, two hybridization $\theta_{1,2}$ and two pairing amplitudes $\Delta_{1,2}$ between bath orbitals, with signs appropriate for describing d-wave superconductivity. This way of parametrizing the bath is not the most general possible, but has been successfully used in the past [48–50]. The 2-site cluster connects the two layers and also contains 6 bath parameters, except that the anomalous part is contained in the hybridization, i.e., it connects the bath sites to the cluster sites, not the bath sites themselves. In order to allow for a relative phase between the pairing on the two layers, the pairing bath parameters $\Delta_{1,2}$ on the square cluster of the second layer are allowed to take complex values, whereas those on the first layer are assumed to be real. Once a converged CDMFT solution is found, the same order parameters $\Delta^{(\ell)}$ as in the previous section are computed.

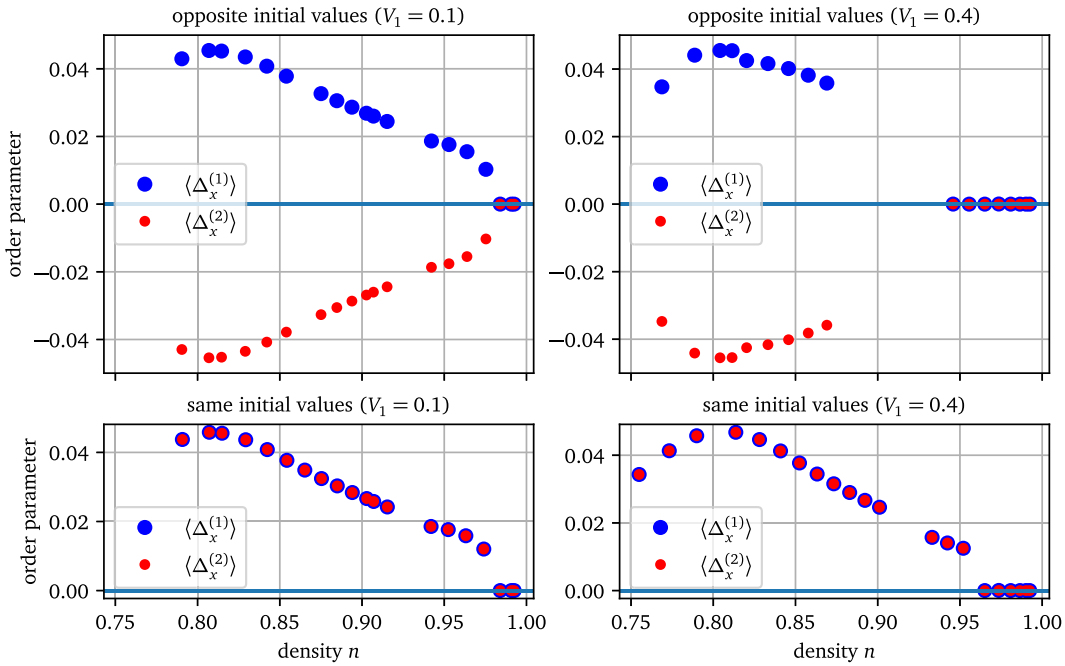

FIG. 9. Order parameter as a function of electron density n, as found in CDMFT, for the two sets of interlayer hopping. The anomalous bath parameters were initially set to have opposite (top) or identical (bottom) signs.

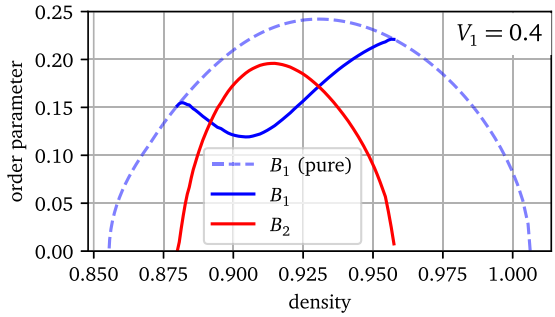

FIG. 10. Same as Fig. 5, but for a unit cell made of two 4-site clusters (one on each layer) plus one 2-site cluster. The TRS-breaking phase is present, but surrounded by the B_1 phase, in contrast to the results of Fig. 5.

Figure 9 shows the results of CDMFT applied to this system, for both intermediate (left) and strong (right) interlayer tunneling. The results depend on the initial set of bath parameters. On the top panels, the bath pairing parameters were initialized with opposite values on the two layers, whereas on the bottom panels, they were initialized with the same values. At intermediate interlayer tunneling ($V_1 = 0.1$), the order parameters stay opposite throughout the doping range if the bath pairings are initialized this way; in other words, if the system is primed in the B_2 representation, it will stay in that representation. At strong interlayer tunneling ($V_1 = 0.4$), this only occurs if doping is large enough. In other words, for doping 12% or less, the system primed in the B_2 representation will either not converge, or converge to a normal solution, indicating its incompatibility with the B_2 initial conditions. On the other hand, if the system is primed in the B_1 representation, then it stays in the B_1 representation, except that, at strong interlayer tunneling, it converges for larger values of doping, and converges to a normal solution at very small doping.

It is thus difficult to discriminate between the B_1 and B_2 representations within CDMFT, which does not have the fine energy resolution that VCA has. Nevertheless, we sense from the above results that the B_1 representation is preferred at low doping and the B_2 representation at higher doping, but a strong interlayer tunneling is needed for that. Also, despite allowing in principle for an arbitrary complex phase between the anomalous bath parameters of the two layers, only the phases 0 and π are found: No state with spontaneous breaking of time reversal is found in CDMFT. A possible explanation is that the main 4-site impurity model in CDMFT is confined to each layer, i.e., the complex, twisted interlayer structure has an impact only through the self-consistency relation. One way to check whether this is a correct explanation is to go back to VCA, this time with the same cluster structure as in CDMFT (two 4-site clusters and one 2-site cluster). The results are shown in Fig. 10. We still observe a TRS-breaking phase between $n = 0.88$ and $n = 0.96$, except that the B_1 representation wins at higher doping, contrary to what was obtained in Sec. III using a 8-site cluster with interlayer tunneling operators within the cluster. This shows that the absence of such operators in the cluster does not preclude the emergence of a TRS-breaking phase. In the case of CDMFT, we are therefore led to blame the lower energy resolution of the method. In studying such systems, it seems that the VCA is a better choice.

VI. CONCLUSIONS

In a one-band Hubbard model for a cuprate bilayer twisted by an angle of 53.13°, the relative phase of the superconducting order parameter in the two layers depends on hole doping away from half-filling. In the underdoped regime, the relative phase vanishes, whereas it is π in the overdoped regime. If the interlayer tunneling is strong, then there is an intermediate phase between those two in which this phase varies continuously from 0 to π. Time reversal symmetry is broken in that intermediate phase, but the topology is trivial, at least as computed from the electron Green function. At intermediate interlayer tunneling, this TRS breaking phase does not exist. These conclusions are reached with the VCA method, using a symmetric 8-site cluster and a 2-site cluster to form the 10-site unit cell, and using similar variational parameters falling in the B_1 and B_2 representations of D_{4h}, the point group of the system. Variants of the VCA procedure using additional Weiss fields for interlayer pairing, or smaller, 4-site clusters without interlayer operators, also produce a TRS breaking phase at strong interlayer tunneling, but no B_2 representation at higher doping. The CDMFT method does not reveal a TRS-breaking field, a fact that we attribute to the lower energy resolution of the method.

It is possible that this TRS breaking phase survives at weaker interlayer tunneling if the twist angle is closer to 45°. Indeed, we naturally expect that a twist closer to 45° would favor the $d_{x^2-y^2} + id_{xy}$ mixed state, maybe enough to compensate a drop in the interlayer coupling. A twist angle of 43.60° corresponds to a unit cell of 58 copper sites [20] and might be amenable to a similar VCA study, albeit markedly more complex numerically. Work in this direction will be necessary in order to assess whether this putative phase is realistic in strong-coupling superconductivity.

ACKNOWLEDGMENTS

Stimulating conservations with A.-M. Tremblay and M. Bélanger are gratefully acknowledged. Computing resources were provided by Compute Canada and Calcul Québec. X.L. is supported by the National Natural Science Foundation of China (Grant No. 11974293) and the Fundamental Research Funds for Central Universities (Grant No. 20720180015). D.S. acknowledges NSERC (Canada) under Grant No. RGPIN-2020-05060.

[1] Y. Cao, V. Fatemi, S. Fang, K. Watanabe, T. Taniguchi, E. Kaxiras, and P. Jarillo-Herrero, Nature (London) **556**, 43 (2018).

[2] Y. Cao, V. Fatemi, A. Demir, S. Fang, S. L. Tomarken, J. Y. Luo, J. D. Sanchez-Yamagishi, K. Watanabe, T. Taniguchi, E. Kaxiras *et al.*, Nature (London) **556**, 80 (2018).

[3] E. Y. Andrei and A. H. MacDonald, Nat. Mater. **19**, 1265 (2020).

[4] S. Carr, D. Massatt, S. Fang, P. Cazeaux, M. Luskin, and E. Kaxiras, Phys. Rev. B **95**, 075420 (2017).

[5] R. Bistritzer and A. H. MacDonald, Proc. Natl. Acad. Sci. USA **108**, 12233 (2011).

[6] J. M. B. Lopes dos Santos, N. M. R. Peres, and A. H. Castro Neto, Phys. Rev. Lett. **99**, 256802 (2007).

[7] G. Tarnopolsky, A. J. Kruchkov, and A. Vishwanath, Phys. Rev. Lett. **122**, 106405 (2019).

[8] D. M. Kennes, M. Claassen, L. Xian, A. Georges, A. J. Millis, J. Hone, C. R. Dean, D. N. Basov, A. N. Pasupathy, and A. Rubio, Nat. Phys. **17**, 155 (2021).

[9] E. C. Regan, D. Wang, C. Jin, M. I. Bakti Utama, B. Gao, X. Wei, S. Zhao, W. Zhao, Z. Zhang, K. Yumigeta *et al.*, Nature (London) **579**, 359 (2020).

[10] Y. Tang, L. Li, T. Li, Y. Xu, S. Liu, K. Barmak, K. Watanabe, T. Taniguchi, A. H. MacDonald, J. Shan, and K. F. Mak, Nature (London) **579**, 353 (2020).

[11] L. Wang, E.-M. Shih, A. Ghiotto, L. Xian, D. A. Rhodes, C. Tan, M. Claassen, D. M. Kennes, Y. Bai, B. Kim *et al.*, Nat. Mater. **19**, 861 (2020).

[12] X. Huang, T. Wang, S. Miao, C. Wang, Z. Li, Z. Lian, T. Taniguchi, K. Watanabe, S. Okamoto, D. Xiao, S.-F. Shi, and Y.-T. Cui, Nat. Phys. **17**, 715 (2021).

[13] X. Liu, Z. Hao, E. Khalaf, J. Y. Lee, Y. Ronen, H. Yoo, D. Haei Najafabadi, K. Watanabe, T. Taniguchi, A. Vishwanath, and P. Kim, Nature (London) **583**, 221 (2020).

[14] Y. Cao, D. Rodan-Legrain, O. Rubies-Bigorda, J. M. Park, K. Watanabe, T. Taniguchi, and P. Jarillo-Herrero, Nature (London) **583**, 215 (2020).

[15] C. Zhang, T. Zhu, S. Kahn, S. Li, B. Yang, C. Herbig, X. Wu, H. Li, K. Watanabe, T. Taniguchi *et al.*, Nat. Commun. **12**, 2516 (2021).

[16] G. Chen, L. Jiang, S. Wu, B. Lyu, H. Li, B. L. Chittari, K. Watanabe, T. Taniguchi, Z. Shi, J. Jung *et al.*, Nat. Phys. **15**, 237 (2019).

[17] G. Chen, A. L. Sharpe, P. Gallagher, I. T. Rosen, E. J. Fox, L. Jiang, B. Lyu, H. Li, K. Watanabe, T. Taniguchi *et al.*, Nature (London) **572**, 215 (2019).

[18] G. Chen, A. L. Sharpe, E. J. Fox, Y.-H. Zhang, S. Wang, L. Jiang, B. Lyu, H. Li, K. Watanabe, T. Taniguchi *et al.*, Nature (London) **579**, 56 (2020).

[19] J. M. Park, Y. Cao, K. Watanabe, T. Taniguchi, and P. Jarillo-Herrero, Nature (London) **590**, 249 (2021).

[20] O. Can, T. Tummuru, R. P. Day, I. Elfimov, A. Damascelli, and M. Franz, Nat. Phys. **17**, 519 (2021).

[21] P. A. Volkov, J. H. Wilson, and J. H. Pixley, arXiv:2012.07860.

[22] Y. Yu, L. Ma, P. Cai, R. Zhong, C. Ye, J. Shen, G. D. Gu, X. H. Chen, and Y. Zhang, Nature (London) **575**, 156 (2019).

[23] S. Y. Frank Zhao, N. Poccia, M. G. Panetta, C. Yu, J. W. Johnson, H. Yoo, R. Zhong, G. D. Gu, K. Watanabe, T. Taniguchi, S. V. Postolova, V. M. Vinokur, and P. Kim, Phys. Rev. Lett. **122**, 247001 (2019).

[24] Q. Li, Y. N. Tsay, M. Suenaga, R. A. Klemm, G. D. Gu, and N. Koshizuka, Phys. Rev. Lett. **83**, 4160 (1999).

[25] Y. Takano, T. Hatano, A. Fukuyo, A. Ishii, M. Ohmori, S. Arisawa, K. Togano, and M. Tachiki, Phys. Rev. B **65**, 140513(R) (2002).

[26] Y. I. Latyshev, A. P. Orlov, A. M. Nikitina, P. Monceau, and R. A. Klemm, Phys. Rev. B **70**, 094517 (2004).

[27] R. A. Klemm, Philos. Mag. **85**, 801 (2005).

[28] Z. Yang, S. Qin, Q. Zhang, C. Fang, and J. Hu, Phys. Rev. B **98**, 104515 (2018).

[29] Y. Zhu, M. Liao, Q. Zhang, H.-Y. Xie, F. Meng, Y. Liu, Z. Bai, S. Ji, J. Zhang, K. Jiang, R. Zhong, J. Schneeloch, G. Gu, L. Gu, X. Ma, D. Zhang, and Q.-K. Xue, Phys. Rev. X **11**, 031011 (2021).

[30] S. Y. F. Zhao, N. Poccia, X. Cui, P. A. Volkov, H. Yoo, R. Engelke, Y. Ronen, R. Zhong, G. Gu, S. Plugge, T. Tummuru, M. Franz, J. H. Pixley, and P. Kim, arXiv:2108.13455.

[31] T. Tummuru, S. Plugge, and M. Franz, Phys. Rev. B **105**, 064501 (2022).

[32] P. A. Volkov, S. Y. F. Zhao, N. Poccia, X. Cui, P. Kim, and J. H. Pixley, arXiv:2108.13456.

[33] X.-Y. Song, Y.-H. Zhang, and A. Vishwanath, Phys. Rev. B **105**, L201102 (2022).

[34] R. S. Markiewicz, S. Sahrakorpi, M. Lindroos, H. Lin, and A. Bansil, Phys. Rev. B **72**, 054519 (2005).

[35] M. Potthoff, Eur. Phys. J. B **32**, 429 (2003).

[36] M. Potthoff, M. Aichhorn, and C. Dahnken, Phys. Rev. Lett. **91**, 206402 (2003).

[37] M. Potthoff, in *DMFT at 25: Infinite dimensions, Lecture Notes of the Autumn School on Correlated Electrons 2014*, edited by E. Pavarini, E. Koch, D. Vollhardt, and A. Lichtenstein (Forschungszentrum Jülich, Germany, 2014).

[38] D. Sénéchal, D. Perez, and M. Pioro-Ladrière, Phys. Rev. Lett. **84**, 522 (2000).

[39] C. Gros and R. Valenti, Phys. Rev. B **48**, 418 (1993).

[40] Indeed, even a single layer is problematic in VCA with a 5-site cluster: The Potthoff functional has discontinuities and no non-trivial solution can be found. Symmetries need to be respected whenever possible.

[41] Z. Wang and S.-C. Zhang, Phys. Rev. X **2**, 031008 (2012).

[42] Z. Wang and S.-C. Zhang, Phys. Rev. B **86**, 165116 (2012).

[43] A. I. Lichtenstein and M. I. Katsnelson, Phys. Rev. B **62**, R9283(R) (2000).

[44] G. Kotliar, S. Y. Savrasov, G. Pálsson, and G. Biroli, Phys. Rev. Lett. **87**, 186401 (2001).

[45] A. Liebsch, H. Ishida, and J. Merino, Phys. Rev. B **78**, 165123 (2008).

[46] D. Sénéchal, in *Many-Body Physics: From Kondo to Hubbard* Vol. 5, edited by E. Pavarini, E. Koch, and P. Coleman (Forschungszentrum Jülich, Germany, 2015) pp. 13.1–13.22.

[47] M. Caffarel and W. Krauth, Phys. Rev. Lett. **72**, 1545 (1994).

[48] S. S. Kancharla, B. Kyung, D. Sénéchal, M. Civelli, M. Capone, G. Kotliar, and A.-M. S. Tremblay, Phys. Rev. B **77**, 184516 (2008).

[49] B. Kyung, D. Sénéchal, and A.-M. S. Tremblay, Phys. Rev. B **80**, 205109 (2009).

[50] A. Foley, S. Verret, A.-M. S. Tremblay, and D. Sénéchal, Phys. Rev. B **99**, 184510 (2019).